Published in final edited form as:
J Biomech. 2015 January 21; 48(2): 310–317. doi:10.1016/j.jbiomech.2014.11.028.

Fracture Healing in Mice Lacking Pten in Osteoblasts: A Micro-Computed Tomography Image-Based Analysis of the Mechanical Properties of the Femur

Caitlyn J. Collins[1], **Juan Vivanco**[1,3], **Scott Sokn**[1], **Bart O. Williams**[2], **Travis A. Burgers**[2], and **Heidi-Lynn Ploeg**[1]

[1]University of Wisconsin-Madison, Department of Mechanical Engineering, Madison, WI

[2]Van Andel Research Institute, Grand Rapids, MI

[3]Universdad Adolfo Ibáñez, Facultad de Ingeniería y Ciencias, Viña del Mar, Chile

Abstract

In the United States, approximately 8 million osseous fractures are reported annually, of which 5-10% fail to create a bony union. Osteoblast-specific deletion of the gene *Pten* in mice has been found to stimulate bone growth and accelerate fracture healing. Healing rates at four weeks increased in femurs from *Pten* osteoblast conditional knock-out mice (Pten-CKO) compared to wild-type mice (WT) of the same genetic strain as measured by an increase in mechanical stiffness and failure load in four-point bending tests. Preceding mechanical testing, each femur was imaged using a Skyscan 1172 micro-computed tomography (μCT) scanner (Skyscan, Kontich, Belgium). The present study used μCT image-based analysis to test the hypothesis that the increased femoral fracture force and stiffness in Pten-CKO were due to greater section properties with the same effective material properties as that of the WT. The second moment of area and section modulus were computed in *ImageJ 1.46* (National Institutes of Health) and used to predict the effective flexural modulus and the stress at failure for fourteen pairs of intact and callus WT and twelve pairs of intact and callus Pten-CKO femurs. For callus and intact femurs, the failure stress and tissue mineral density of the Pten-CKO and WT were not different; however, the section properties of the Pten-CKO were more than twice as large 28 days post-fracture. It was therefore concluded, when the gene *Pten* was conditionally knocked-out in osteoblasts, the resulting increased bending stiffness and force to fracture were due to increased section properties.

Corresponding author: Heidi-Lynn Ploeg, Associate Professor, Dept. of Mechanical Engineering University of Wisconsin-Madison, 1513 University Avenue, Room 3043, Madison, Wisconsin 53706, Tel: (608) 262-2690, Fax: (608) 265-2316, ploeg@engr.wisc.edu.

Conflict of Interest Statement: No conflict exists for any of the authors that would result in a bias in the research.

Keywords

fracture healing; mouse femur; Pten gene; micro computed tomography image-based analysis; section properties; mechanical properties; four-point bend testing

Introduction

The incidence of delayed fracture healing, or non-union, is estimated to occur in 5-10% of fractures (Hardwood et al., 2010). In elderly persons with osteoporosis, non-union rates can be upwards of 30% (Parker et al., 2007).

Though much of the research behind treatment for bone frailty and fracture healing has focused on physiological and growth-factor treatments (Kristiansen et al., 1997; Lieberman et al., 2002; Govender et al., 2002), roughly 60-70% of the variation in person-to-person bone mineral density has been shown to be hereditary. Studies have found mechanosensitivity to have a genetic basis (Akhter et al., 1998; Kodama et al., 2000; Robling and Turner, 2002; Burgers and Williams, 2013). Therefore, understanding the molecular and cellular signaling pathways targeted by the genes governing bone frailty and fracture healing has potential for influencing treatments affecting bone mass accumulation and reducing fracture rates.

One such pathway is the phosphatidylinositol 3-kinase (PI3K)-Akt pathway which leads to osteoblast differentiation (Cantley, 2002; Yuan and Cantley, 2008; Hers et al., 2011). Within this pathway, the *PTEN* gene (phosphatase and tensin homologue on human chromosome 10) encodes the Pten protein and negatively regulates activation of Akt. If Pten is removed or blocked, Akt is activated indefinitely, allowing continual cell proliferation. Mice carrying a Cre-mediated osteoblast-specific deletion of the *Pten* gene ($Ocn\text{-}cre^{tg/+}$; $Pten^{flox/flox}$) were shown to continually grow bone throughout their 15-month lifespan (Liu et al., 2007). *Pten* conditional knock-out mice (Pten-CKO) maintained normal body size, but developed larger bone volume with increases in cortical and trabecular bone compared to wild-type mice (WT). Increased mineral apposition and decreased osteoblast apoptosis rates were also reported.

Improved fracture healing was found in a study which used four-point bending mechanical testing to assess the healing rate of femoral fractures in Pten-CKO (Burgers et al., 2013). At 28 days post-fracture (PF) Pten-CKO had significantly higher bending stiffness (K) and peak force to failure (F_{max}) than WT. Pten-CKO maintained a larger callus bone volume up to 21 days PF than WT, but callus tissue mineral density was only found to be significantly greater at 14 days PF. Elevated osteoblastic and osteoclastic activity in the callus of Pten-CKO were also reported. These results suggest that the increased resistance to bending in Pten-CKO femurs may be due to larger section properties while material properties of the bone tissue may be equivalent to WT femurs. Further evaluation of the relative contributions to the increased bending resistance of Pten-CKO femurs is necessary to better understand the effects of blocking the *Pten* gene, motivating the current study.

Bone structural properties, such as stiffness and strength, depend on geometry and the material within (Spatz et al., 1996; Jämsä et al., 1998; Brodt et al., 1999; Akhter et al., 2001; Jiang et al., 2005; Schriefer et al., 2005). The simplest approach to determine contributions to a bone's mechanical behavior under a given load configuration is to assume a simplified geometry based on measured bone dimensions (Indrekvam et al., 1991; Keller et al., 1986; Levenston et al., 1994). Medical image-based methods have become increasingly common because they provide accurate section geometry, and distinguish between section and material contributions to structural properties using analytical methods based on classical mechanics (Levenston et al., 1994; Morgan et al., 2009; Nyman et al., 2009; O'Neill et al., 2012). Finally, medical image-based finite element modeling (FEM) (Weiss et al., 2012; Shefelbine et al., 2005) is a numerical method that predicts the mechanical response of bone under load by modeling the bone's geometry, mechanical properties, and boundary conditions. Although FEM is arguably the most accurate and informative of these methods, it is also the most complex, requiring more time and resources. Current medical imaging technology and software available at no cost from the National Institutes of Health (NIH) make the determination of section versus material contributions to bone's mechanical response to a given load configuration relatively efficient. The present study, therefore, used medical image-based analytical methods to determine the mechanical response of mouse femurs under four-point bending.

Based on findings of previous studies, the authors of the present study hypothesized that the greater K and F_{max} of Pten-CKO compared to WT femurs were due to an increase in section properties. The purpose of the current study was to determine if Pten-CKO produced bone with greater section properties than and equivalent effective material properties to WT.

Materials and Methods

The previous study, approved by the Institutional Animal Use and Care Committee at the Van Andel Research Institute, Grand Rapids, MI, used 96 mice to investigate the influence of Pten on biomechanical properties of the femur during fracture healing (Burgers et al., 2013). Of these mice, the 66 subjected to mechanical testing and micro-computed tomography (μ-CT) imaging were the focus of the present study.

A mid-diaphyseal fracture was induced in mice 11 to 12 weeks old using the procedure outlined by Burgers and co-workers (2013). Fractures identified as oblique, comminuted, or incomplete were excluded from further mechanical tests. As a result, 21 callus femurs (10 WT and 11 Pten-CKO) were omitted leaving 66 intact and 45 callus femurs available for mechanical testing.

Mice were allowed to freely ambulate until sacrifice at 7, 14, 21, or 28 days PF. Upon sacrifice, the stabilizing intramedullary needles were removed from callus femurs and all femurs were excised, cleaned of soft tissue, and stored at -20°C in saline-saturated gauze. All femurs were scanned in saline at room temperature using a Skyscan 1172 high-resolution μ-CT scanner (Skyscan, Kontich, Belgium) with 13.3 μm cubic voxel sizes. Within the scanner, femurs were oriented such that voxel depth was roughly parallel to the long axis of the bone. Two density calibration phantoms (0.25 g/cm^3 and 0.75 g/cm^3) were

included in each scan to determine equation coefficients for calibrated density-specific analyses. Images were reconstructed using accompanying Skyscan software and imported as Digital Imaging and Communications in Medicine (DICOM) files into the medical image processing software Mimics (Mimics ×64 14.11, Materialise, Ann Arbor, MI). The original μ-CT data were compressed to preserve working memory space resulting in non-cubic voxels with pixel height and width of the original resolution, 13.3 μm, and voxel depth of 26.6 μm.

After μ-CT scanning, the bones were stored at -20°C until allowed to equilibrate to room temperature in saline for 30 minutes prior to mechanical testing. Succeeding equilibration, a standard four-point bend testing procedure was performed using a TestResources 570L axial-torsional screw-driven testing system (TestResources, Shakopee, MN) with displacement rate of 0.005 mm/s. The distances between the lower and upper supports were 8.0 and 4.0 mm, respectively (Figure 1). The supports had radii of curvature of 0.5 mm at each point of contact with the femur. Displacement was applied by the upper supports in the anterior-posterior direction such that the anterior of the femur was in compression and the posterior was in tension. Callus bones were positioned so that the callus was centered between the upper supports. Intact bones were similarly positioned on the lower supports such that the head of each intact femur matched the position of the head of the contralateral callus femur. To establish even contact on the anterior and posterior surfaces of the femur, the lower support was allowed to pivot about the transverse axis (normal to the plane of Figure 1). Force and displacement were directly measured from the load cell and crosshead, respectively.

In the present research, μ-CT image-based mechanical analysis was performed on fourteen pairs of intact and callus WT (7 male and 7 female) and twelve pairs of intact and callus Pten-CKO (5 male and 7 female) femurs, from 14, 21, and 28 days PF, summarized in Table 1. Day 7 mice were excluded from analysis as they were too compliant during mechanical testing. An additional pair of intact and callus WT femurs from 14 days PF, excluded from mechanical testing due to fracture upon intramedullary pin removal, was included in the analysis. Prior to analysis, each μ-CT image was re-oriented from the scanned to the approximate bending test orientation, within Mimics, such that the cross-section within the transverse plane was perpendicular to the long axis of the bone. DICOM files of each re-sliced image sequence were exported and processed using *ImageJ 1.46* NIH software (Rasband, 1997). A Hounsfield Unit (HU) thresholding range, representative of bone (226-3071 HU (Otsu, 1979; Hangertner, 2005; Komatsu et al., 2010)), and scan specific density calibration equation coefficients were applied to the *slice geometry* macro of *BoneJ*, a plugin for *ImageJ*, to determine section and material properties of each μ-CT slice along the long axis of each femur: tissue mineral density (*TMD*), cross-sectional area (*A*), minimum second moment of area (I_{min}) and minimum section modulus (z_{min}) (Doube et al., 2010). After thresholding, bone volume (*BV*) was calculated from the sum of the areas (*A*) by the slice thickness across the center 4 mm of each bone. *TMD*, *A*, I_{min} and z_{min} were each averaged across the center 4 mm of each bone, the portion between the upper supports during testing, to filter noise from the raw data.

K was calculated using linear regression within the linear region of the force versus deflection curve, represented by Equation 1, where *F* is measured force and δ is the applied deflection of the upper supports. Section properties were combined with F_{max} and *K* to predict maximum stress at failure (σ_{max}) and effective flexural modulus (E_{eff}) of the bones using Hooke's law and Euler-Bernoulli's classic beam bending theory for symmetric beams in pure bending (Equations 2, 3 & 4). z_{min} and I_{min}, were used in the predictions of σ_{max} and E_{eff} as they were repeatable and fair representations of a section transverse to the bending plane of the four-point bend test. In these equations, *a* (= 2 mm) is the constant moment arm from the upper to the lower support, *x* (= a) is the position at which deflection was measured, *L* (= 8 mm) is the distance between the lower supports, and *G* is the shear modulus.

$$K=\frac{F}{\delta} \quad \text{Equation (1)}$$

$$E_{\text{eff}}=\frac{a(3Lx-3x^2-a^2)\boldsymbol{K}}{12\boldsymbol{I}_{\min}} \quad \text{Equation (2)}$$

$$\sigma_{\max}=\frac{a\boldsymbol{F}_{\max}}{2\boldsymbol{Z}_{\min}} \quad \text{Equation (3)}$$

$$slenderness=\frac{\boldsymbol{GAL}}{E_{\text{eff}}\boldsymbol{I}_{\min}} \quad \text{Equation (4)}$$

To quantify error in *K* due to localized deflection, Hertz contact stress equations (Roark et al., 2001) were used to estimate deformation (*y*) of the intact WT and Pten-CKO femurs at the supports. λ is 0.822, a geometric parameter, C_E is the equivalent modulus, K_D is the effective diameter (Equations 5, 6, & 7). The contact surfaces of the supports and the intact WT and Pten-CKO femurs were idealized as perpendicular cylinders with diameters of 1.0 mm (D_1) and 2.3 mm and 2.6 mm (D_2), respectively. Elastic moduli of 200 GPa (E_1) and E_{eff} (E_2) were used for the steel support and the femurs, respectively. Poisson's ratios of 0.3 were assumed for the steel support (v_1) and bones (v_2).

$$y=\lambda^3\sqrt{\frac{F^2C_E^2}{K_D}} \quad \text{Equation (5)}$$

$$K_D=\frac{D_1D_2}{D_1+D_2} \quad \text{Equation (6)}$$

$$C_E=\frac{1-v_1^2}{E_1}+\frac{1-v_2^2}{E_2} \quad \text{Equation (7)}$$

A mixed effects linear regression analysis with group, leg, and numeric time as fixed effects and mouse ID as a random effect was used to determine the effects of conditional deletion of *Pten* in osteoblasts with time after fracture on F_{max}, K, I_{min}, z_{min}, E_{eff}, and σ_{max}. The full model was first fit with 3-way interaction and all 2-way interactions. If the 3-way interaction was insignificant ($p>0.05$) it was removed and all 2-way interactions were examined and removed in order of least significant first and so on until all interactions were removed or only significant interactions remained. A repeated measures analysis of variance (RM-ANOVA) was applied at each time point to determine if any significant differences existed between callus and intact femurs of each group for corresponding days PF. If significance was found, pairwise comparisons were examined and Holm adjusted p-values were calculated to account for type-I error inflation. Log-transformations were applied to z_{min} and I_{min} data and a square-root transformation was applied to E_{eff} data to ensure that the residuals of each model sufficiently met the assumptions of being normally distributed about zero with variance independent from the response variable. Confidence intervals (CIs) which extended below the natural limit for each response variable were truncated to zero. All statistical analyses were conducted with the software R 2.15 (R Foundation for Statistical Computing, Vienna, Austria). Sex was not investigated in the present study as Burgers and co-workers (2013) found sex to be insignificant for K, F_{max}, and healing rate.

Results

μ-CT Images

Intact Pten-CKO femurs were larger in size and appeared more porous compared to WT at 28 days PF (Figure 2). Increased mineralization and reduced callus size can be seen from 14 to 28 days PF in both callus Pten-CKO and WT femurs (Figure 3).

Maximum Force, Maximum Stress at Failure, and Minimum Section Modulus

F_{max} remained constant in intact femurs of Pten-CKO and WT over the course of the study (slope=1.1, 95% CI: -3.5, 5.7, p=0.66) (Figure 4a). F_{max} increased throughout healing in callus Pten-CKO and WT femurs with a slope 10.8 (95% CI: 4.3, 17.4, p=0.004) units greater than intact femurs. By 28 days PF, F_{max} in callus Pten-CKO and WT femurs were 23% (p=0.006) and 32% less than their corresponding intact femurs, respectively. At 28 days PF, F_{max} of intact and callus Pten-CKO femurs were 88% (p=0.001) and 65% (p=0.017) larger than corresponding WT femurs, respectively.

σ_{max} remained constant in the intact femurs of Pten-CKO and WT over the course of the study (slope=4.8, 95% CI: -1.9, 11.5, p=0.17) (Figure 4b). σ_{max} increased over time in callus Pten-CKO and WT femurs with a slope 10.7 (95% CI: 1.3, 20.1, p=0.036) units greater than intact femurs. σ_{max} of callus Pten-CKO and WT femurs were significantly less than intact femurs for all days PF (RM-ANOVA $p<0.001$). By 28 days PF, σ_{max} in callus Pten-CKO and WT femurs were 63% and 62% less than their corresponding intact femurs, respectively. σ_{max} of the intact and callus Pten-CKO femurs were not statistically different from their respective WT femurs.

No significant differences were found in z_{min} between days 14 and 28 PF for either intact or callus femurs of Pten-CKO or WT (p=0.56) (Figure 4c). z_{min} of intact and callus Pten-CKO femurs were nearly twice as large as their respective WT counterparts for all days PF. z_{min} of callus femurs of Pten-CKO and WT (p=0.017) were more than twice as large as their respective contralateral intact femurs.

Bending Stiffness, Effective Flexural Modulus, and Minimum Second Moment of Area

K of callus Pten-CKO femurs increased with time (p=0.010) (Figure 5a). No significant change in *K* of callus WT femurs was found with time (p>0.05). At 28 days PF, *K* of callus Pten-CKO and WT femurs were 46% and 29% (p=0.034) less than their corresponding intact femurs, respectively. Further, callus Pten-CKO femurs were 92% stiffer than callus WT femurs; and, intact Pten-CKO femurs were 46% stiffer than intact WT femurs.

E_{eff} increased with time in callus Pten-CKO and WT femurs (p=0.002) (Figure 5b). By day 28 PF, E_{eff} of callus Pten-CKO and callus WT femurs were a sixth (p<0.05) and a seventh (p<0.05) of their respective intact femurs. No significant differences were found in time between E_{eff} of callus Pten-CKO and callus WT femurs. By day 28 PF, E_{eff} of intact Pten-CKO femurs was 40% less (p<0.05) than intact WT femurs.

No significant differences were found in I_{min} between days 14 and 28 PF for either intact or callus femurs of the Pten-CKO or WT (p=0.15) (Figure 5c). I_{min} of intact and callus Pten-CKO femurs were more than twice as large as their respective WT counterparts (p<0.05). I_{min} of callus femurs of Pten-CKO and WT were roughly four times larger than their respective contralateral intact femurs (p<0.05).

Bone Volume and Tissue Mineral Density

No significant changes in *BV* were found over time in callus or intact femurs of Pten-CKO or WT (p=0.85) (Figure 6a). By 28 days PF, *BV*s of intact and callus Pten-CKO femurs were nearly twice as large as their respective WT counterparts (p<0.01); and, *BV*s of callus femurs of Pten-CKO and WT were roughly two times larger than their respective intact femurs (p<0.01). *TMD* of intact femurs of Pten-CKO and WT increased with time (slope=0.06, 95% CI: 0.01, 0.10, p=0.019) (Figure 6b). *TMD* of the callus femurs of Pten-CKO and WT increased with time with a slope 0.04 (95% CI: 0.02, 0.07, p=0.005) units larger than intact femurs. *TMD* of callus Pten-CKO femurs was significantly less than intact Pten-CKO femurs at 14 (p=0.009) and 21 (p=0.009) days PF. *TMD* of callus WT femurs was significantly less than intact WT femurs at 14 (p=0.002), 21 (p=0.010), and 28 (p=0.002) days PF such that *TMD* of callus WT femurs was 11% less than respective intact femurs at 28 days PF.

Discussion

The present study was performed to test the hypothesis that greater *K* and F_{max} of Pten-CKO compared to WT femurs were due to an increase in section properties. This was achieved through murine fracture models, enabling the comparison between intact and healing bone and providing a means to track time-dependent changes in mechanical and effective material properties.

Several limitations in the study are acknowledged. Calculations of σ_{max} and E_{eff} followed assumptions of Hooke's Law and Euler-Bernoulli beam bending theory including linearly elastic, homogeneous, and isotropic material, despite bone's nonlinear, viscoelastic, heterogeneous, and anisotropic properties. Any misrepresentation of material property was standardized since the simplified material model was applied to all femurs. More complex material models can be applied when using FEM, but the present study sought to employ methods which were less costly in time and resources. Although tests were to failure, *K* was determined in the linear region. Four-point bending produces a state of pure bending between the upper supports generating a uniaxial stress state. As a result, the estimated mechanical properties are oriented with the femoral axis. The length-to-diameter ratio of the femurs was roughly 5:1, smaller than recommended for negligible shear deformation (Spatz et al., 1996). The *slenderness* of the femurs, however, indicated a less than 5% overestimation of *K*. Deflection of the femur was measured from crosshead motion; therefore, it included machine compliance and local deformations at the supports. Machine compared to femur compliance was small; however, local deformations at support contacts were large. The Hertz contact analysis predicted 25-49% underestimation of *K*. *K* of Pten-CKO femurs suffered larger underestimations than WT. The present study was limited to μCT data to calculate all section properties; therefore, calculations did not account for the contribution of organic constituents, such as collagen.

A standardized method was used to initiate fracture in Pten-CKO and WT, but the number of omitted callus femurs indicates a lack of reliability in the method. The resultant small sample sizes at certain days PF may have compromised statistical power causing a Type II error. For example, increase in *K* and E_{eff} of callus WT femurs with time was not significant; whereas, a significant increase was found in callus Pten-CKO femurs.

In contrast to results of previous research (Liu et al., 2007; Burgers et al., 2013), no significant difference in *TMD* between Pten-CKO and WT femurs was found. Liu and co-workers (2007) found significantly higher whole body areal bone mineral density in Pten-CKO than WT measured with dual energy x-ray absorptiometry (DXA) at three months of age. Burgers and co-workers (2013) only reported a significant difference in callus tissue mineral density of callus WT and Pten-CKO femurs at day 14 PF. The different findings in comparing density between Pten-CKO and WT may be due, in part, to methodological size error inherent to DXA and size disparity between Pten-CKO and WT femurs.

In agreement with previous studies (Liu et al., 2007; Burgers et al., 2013), section properties were larger in Pten-CKO femurs than their WT counterparts (Figures 2, 4c, 5c). Improved fracture healing was found in Pten-CKO as measured by a lack of significant difference between intact and callus Pten-CKO femurs at 28 days PF (Figure 6b).

Results of intact and callus WT and Pten-CKO femurs demonstrated direct proportionality of F_{max} to σ_{max} and z_{min} (Figure 4a-c). In callus femurs of both groups, F_{max} and σ_{max} were found to increase with time from days 14 to 28 PF but remained significantly less than respective intact femurs. In contrast, z_{min} of callus femurs for both groups did not change and were found to be nearly twice as large as their respective intact femurs (Figure 4c). Increase in F_{max} with time, therefore, was due to increase in σ_{max} with time. Proportional

differences in F_{max}, σ_{max}, and z_{min} of callus compared to intact femurs for both groups showed that lower F_{max} of callus femurs was due to a lower σ_{max} despite higher z_{min}. F_{max} was larger in Pten-CKO than WT femurs due to larger z_{min} with no significant difference in σ_{max}, for both callus and intact femurs (Figure 4a-c). Therefore, increasing F_{max} of the callus femurs was due to healing bones' increasing σ_{max}, and larger F_{max} of Pten-CKO compared to WT femurs was primarily due to their larger z_{min}.

Results of intact and callus WT and Pten-CKO femurs demonstrated direct proportionality of K to E_{eff} and I_{min}. After 28 days, K and E_{eff} of callus femurs of both WT and Pten-CKO remained lower than intact, despite twice larger I_{min} in Pten-CKO femurs. Increase in K of callus Pten-CKO femurs with time was due to a corresponding increase in E_{eff} (Figure 5a,b). Pten-CKO femurs were stiffer than WT due to larger I_{min} (Figure 5a,c). There was no difference in E_{eff} between callus femurs of either group. Contradicting the larger structural and geometric stiffness, E_{eff} of Pten-CKO femurs were found to be lower than WT. E_{eff} may have been smaller in intact Pten-CKO than intact WT because of larger contact deformations under the supports. In summary, increasing K of callus Pten-CKO femurs in time was due to healing bones' increasing E_{eff}, and larger K of Pten-CKO compared to WT femurs was due primarily to larger I_{min}.

Conclusion

Pten-CKO were found to produce femurs with the same σ_{max} as WT. Thus, increased K and F_{max} of Pten-CKO were due to increased section properties and not to increased material properties. The presented study distinguished between the contributions of material and section properties to femoral bending resistance. Further, the present study supports medical image-based analytical methods to assess callus mechanical properties during fracture healing.

Acknowledgments

The authors thank the members of the Mason and Williams labs at Van Andel Research Institute, Grand Rapids, MI (VARI) for their assistance; Martin Hoffmann, Mike Morris, and DJ Scholten for assisting on surgeries and fractures; VARI's vivarium staff for outstanding animal husbandry; Martin Alvarado for CT scanning bones; Will Ault and Morgan Schneider for their assistance in processing the CT data; and Scott Hetzel for his help with the statistical analysis.

Funding was provided by the University of Wisconsin-Madison Graduate School, the Van Andel Research Institute, and was supported by United States National Institutes of Health grant AR053293 (BOW). The funders had no role in study design, data collection and analysis, decision to publish, or preparation of the manuscript.

References

Akhter M, Cullen D, Pedersen E, Kimmel D, Recker R. Bone response to in vivo mechanical loading in two breeds of mice. Calcif Tissue Int. 1998; 63(5):442–449. [PubMed: 9799831]

Akhter M, Cullen D, Gong G, Recker R. Bone biomechancial properties in prostaglandin EP1 and EP2 knockout mice. Bone. 2001; 29(2):121–125. [PubMed: 11502472]

Brodt M, Ellis C, Silva M. Growing C57Bl6 Mice Increase Whole Bone Mechanical Properties by Increasing Geometric and Material Properties. Journal of Bone and Mineral Research. 1999; 14(12): 2159–2166. [PubMed: 10620076]

Burgers T, Hoffmann M, Collins C, Zahatnansky J, Alvarado M, Morris M, Sietsema D, Mason J, Jones C, Ploeg H, Williams B. Mice lacking Pten in osteoblasts have improved intramembranous and late endochondral fracture healing. PLoS One. 2013; 8(5):1–21.

Burgers T, Willaims B. Regulation of the Wnt/β-catenin signaling within and from osteocytes. Bone. 2013; 54:244–249. [PubMed: 23470835]

Cantley L. The Phosphoinositide 3-Kinase Pathway. Science. 2002; 296(5573):1655–1657. [PubMed: 12040186]

Doube M, Kłosowski M, Arganda-Carreras I, Cordelières F, Dougherty R, Jackson J, Schmid B, Hutchinson J, Shefelbine S. BoneJ: Free and extensible bone image analysis in ImageJ. Bone. 2010; 47(6):1076–1079. [PubMed: 20817052]

Govender S, Csimma C, Genant H, Valentin-Opran A, Amit Y, Arbel R, Aro H, Atar D, Bishay M, Borner M, Chiron P, Choong P, Cintas J, Courtenay B, Feibel R, Geulette B, Gravel C, Haas N, Raschke M, Hammacher E, van der Velde D, Hardy P, Holt M, Josten C, Ketterl R, Lindeque B, Lob G, Mathevon H, McCoy G, Marsh D, Miller R, Munting E, Oevre S, Nordsletten L, Patel A, Pohl A, Rennie W, Reynders P, Rommens P, Rondia J, Rossouw W, Daneel P, Ruff S, Ruter A, Santavirta S, Schildhauer T, Gekle C, Schnettler R, Segal D, Seiler H, Snowdowne R, Stapert J, Taglang G, Verdonk R, Vogels L, Weckbach A, Wentzensen A, Wisniewski T. Recombinant human bone morphogenetic protein-2 for treatment of open tibial fractures: a prospective, controlled, randomized study of four hundred and fifty patients. J Bone Joint Surg Am. 2002; 84-A(12):2123–2134. [PubMed: 12473698]

Hangartner T. Thresholding technique for accurate analysis of density and geometry in QCT, pQCT and microCT images. Journal of Musculoskeletal and Neuronal Interactactions. 2007; 7:9–16.

Hardwood P, Newman J, Michael A. (ii) An update on fracture healing and nonunion. Orthopaedics and Trauma. 2010; 24(1):9–23.

Hers I, Vincent E, Tavaré J. Akt signaling in health and disease. Cellular Signalling. 2011; 23(1): 1515–1527. [PubMed: 21620960]

Hugunin K, Fry C, Shuster K, Nemzek J. Effects of tramadol and buprenorphine on select immunologic factors in a cecal ligation and puncture model. Shock. 2010; 34:250–260. [PubMed: 20803785]

Indrekvam K, Schnell Husby O, Gjerdet N, Engester L, Langeland N. Age-dependent mechanical properties of rat femur. Acta Orthopaedica Scandinavica. 1991; 62(3):248–252. [PubMed: 2042467]

Jämsä T, Jalovaara P, Peng Z, Väänänen H. Comparison of three-point bending test and peripheral quantitative computed tomography analysis in the evaluation of the strength of mouse femur and tibia. Bone. 1998; 23(2):155–161. [PubMed: 9701475]

Jiang Y, Zhao J, Liao E, Dai R, Wu X, Genant H. Application of micro-CT assessment of 3-D bone microstructure in preclinical and clinical studies. J Bone Miner Metab. 2005; 23(Suppl):122–131. [PubMed: 15984427]

Keller T, Spengler D, Carter D. Geometric, elastic, and structural properties of maturing rat femora. Journal of Orthopaedic Research. 1986; 4:57–67. [PubMed: 3950809]

Kodama Y, Umemura Y, Nagasawa S, Beamer W, Donahue L, Rosen C, Baylink D, Farley J. Exercise and mechanical loading increase periosteal bone formation and whole bone strength in C57BL/6J mice but not in C3H/Hej mice. Calcif Tissue Int. 2000; 66(4):298–306. [PubMed: 10742449]

Komatsu D, Mary M, Schroeder R, Robling A, Turner C, Warden S. Modulation of Wnt signaling influences fracture repair. Journal of Orthopaedic Research. 2010; 28:928–936. [PubMed: 20063381]

Kristiansen T, Ryaby J, McCabe J, Frey J, Roe L. Accelerated healing of distal radial fractures with the use of specific, low-intensity ultrasound. A multicenter, prospective, randomized, double-blind, placebo-controlled study. J Bone Joint Surg Am. 1997; 79(7):961–973. [PubMed: 9234872]

Levenston M, Beaupre G, van der Meulen M. Improved method for analysis of whole bone torsion tests. Journal of Bone and Mineral Research. 1994; 9(9):1459–1465. [PubMed: 7817831]

Lieberman J, Daluiski A, Einhorn T. The role of growth factors in the repair of bone. Biology and clinical applications. J Bone Joint Surg Am. 2002:1032–1044. [PubMed: 12063342]

Liu X, Bruxvoort K, Zylstra C, Liu J, Cichoowski R, Faugere M, Bouxein M, Wan C, Williams B, Clemens T. Lifelong accumulation of bone in mice lacking *Pten* in osteoblasts. PNAS. 2007; 104(7):2259–2464. [PubMed: 17287359]

Morgan E, Mason J, Chien K, Pfeiffer A, Barnes G, Einhorn T, Gerstenfeld L. Micro-computed tomography assessment of fracture healing: Relationships among callus structure, composition, and mechanical function. Bone. 2009; 44:335–344. [PubMed: 19013264]

Nikolaou V, Efstathopoulos N, Kontakis G, Kanakaris N, Giannoudis P. The influence of osteoporosis in femoral fracture healing time. Injury. 2009; 40(6):663–668. [PubMed: 19324360]

Nyman J, Steve M, Satyawan J, Alfred M, Toshitaka Y, Gregory R, Gloria E. Quantitative measures of femoral fracture repair in rats derived by micro-computed tomography. Journal of Biomechanics. 2009; 42(7):891–897. [PubMed: 19281987]

O'Neill K, Stutz C, Mignemi N, Burns M, Murry M, Nyman J, Schoenecker J. Micro-computed tomography assessment of the progression of fracture healing in mice. Bone. 2012; 50(6):1357–1367. [PubMed: 22453081]

Otsu N. A threshold selection method from gray-level histograms. IEEE Transactions on System, Man and Cybernetics. 1979; 8:62–66.

Parker M, Raghavan R, Gurusamy K. Incidence of fracture-healing complications after femoral neck fractures. Clinical Orthopaedics and Related Research. 2007; 458:175–179. [PubMed: 17224836]

Roark, R.; Young, W.; Budynas, R. Roark's Formulas for Stress and Strain. McGraw Hill Professional; New York City: 2001. p. 702-703.

Rasband, W. ImageJ. U S National Institutes of Health; 1997-2012. http://imagej.nih.gov/ij/

Robling A, Turner C. Mechanotransduction in Bone: Genetic Effects on Mechanosensitivity in Mice. Bone. 2002; 31(5):562–569. [PubMed: 12477569]

Shefelbine S, Simon U, Claes L, Gold A, Gabet Y, Bab I, Muller R, Augat P. Prediction of fracture callus mechanical properties using micro-CT images and voxel-based finite element analysis. Bone. 2005; 36:480–488. [PubMed: 15777656]

Schriefer J, Robling A, Warden S, Fournier A, Mason J, Turner C. A comparison of mechanical properties derived from multiple skeletal sites in mice. Journal of Biomechanics. 2005; 38(3):467–475. [PubMed: 15652544]

Spatz H, O'Leary E, Vincent J. Young's moduli and shear moduli in cortical bone. Proceedings: Biological Sciences. 1996; 263(1368):287–294.

Weis J, Granero-Molto F, Myers T, Longobardi L, Spafnoli A, Miga M. Comparison of microCT and an inverse finite element approach for biomechanical analysis: Results in a MSC therapeutic system for fracture healing. Journal of Biomechanics. 2012; 45(12):2164–2170. [PubMed: 22766379]

Yuan T, Cantley L. PI3K pathway alterations in cancer : variations on a theme. Oncogene. 2008; 27:5497–5510. [PubMed: 18794884]

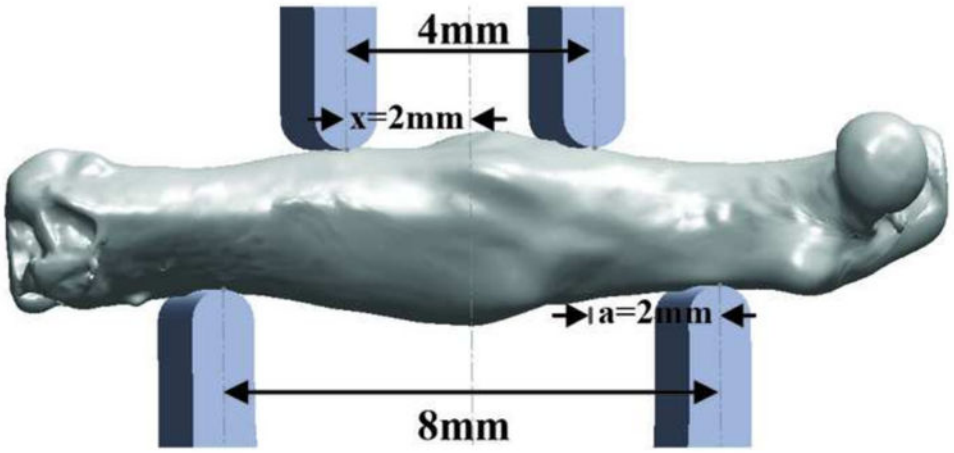

Figure 1.

Three dimensional models of four-point bending apparatus with distances between the upper and lower supports labeled and a callus Pten-CKO mouse femur from 28 days PF between the upper and lower supports. The moment arm from the upper support to the lower support, *a*, and the position at which deflection was measured, *x*, are also labeled.

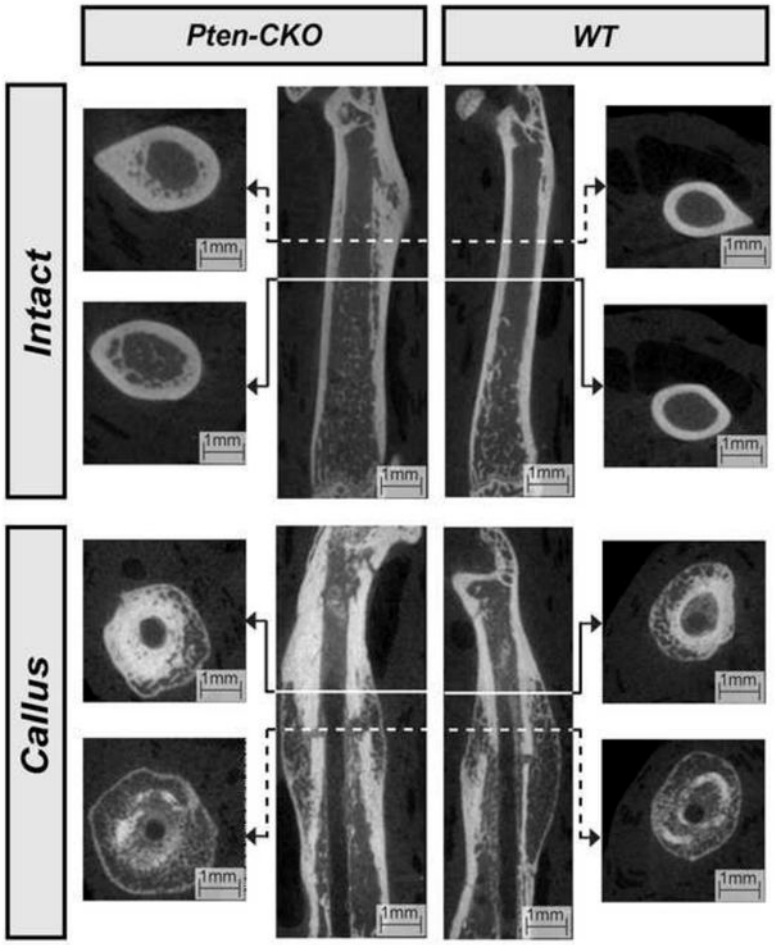

Figure 2.

Sagittal (Center) and transverse (Peripheral) μ-CT images of proximal and mid-diaphyseal sections, as indicated, of select intact (Top) and callus (Bottom) WT (Right) and Pten-CKO (Left) femurs at day 28 PF. Intact Pten-CKO femurs were larger in size and appeared more porous compared to intact WT femurs at day 28 PF.

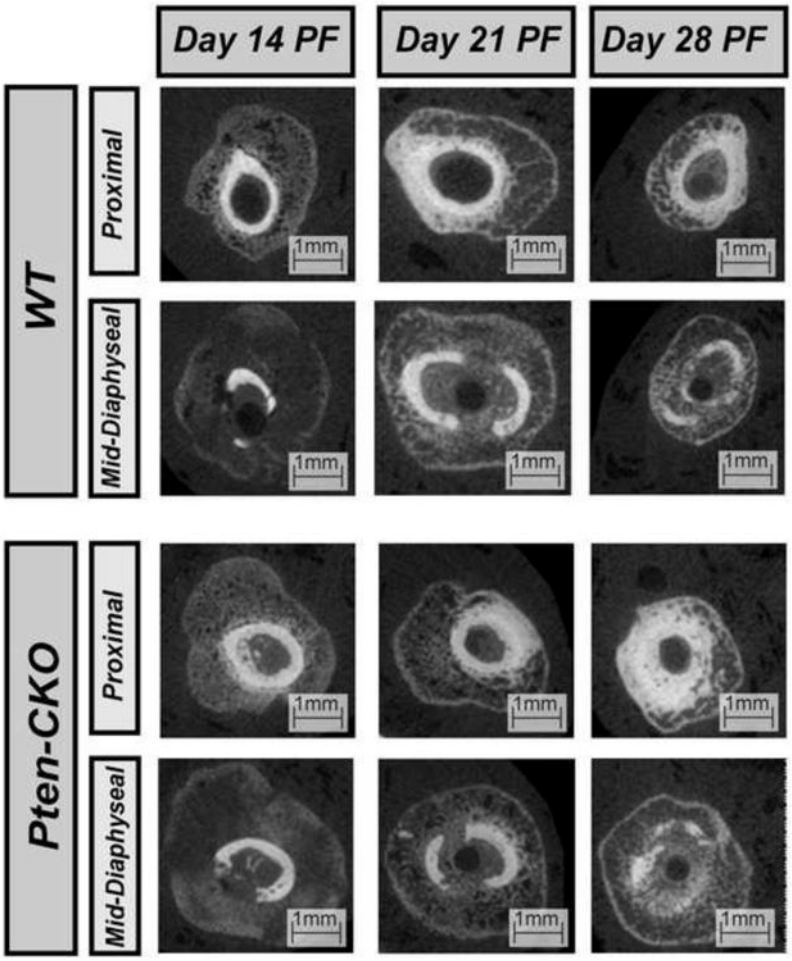

Figure 3.

Transverse μ-CT images of the proximal and mid-diaphyseal sections of select WT callus (Top) and Pten-CKO callus (Bottom) femurs at days 14, 21, and 28 PF. Increased mineralization and a reduction in callus size can be seen by day 28 PF in both callus Pten-CKO and WT femurs.

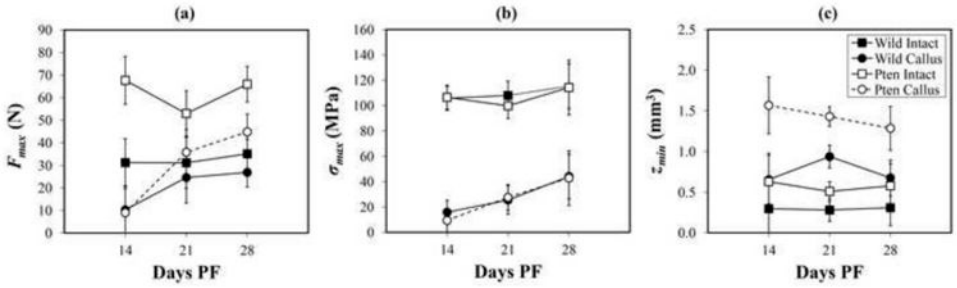

Figure 4.

a. Maximum force to failure, F_{max}, versus days PF, with 95% CIs labeled. No significant increase in F_{max} was found over time in intact femurs of both Pten-CKO and WT (slope=1.1, 95% CI: -3.5, 5.7, p=0.66). F_{max} increased throughout healing in callus Pten-CKO and WT femurs with a slope 10.8 units higher than intact femurs (95% CI: 4.3, 17.4, p=0.004). By day 28 PF, F_{max} in callus Pten-CKO and WT femurs were 23% (p=0.006) and 32% less than their corresponding intact bones, respectively. At 28 days PF, F_{max} of intact and callus Pten-CKO femurs were significantly larger than their WT counterparts (p=0.001, p=0.017).

b. Maximum bending stress, σ_{max}, versus days PF, with 95% CIs labeled. No significant increase in σ_{max} was found over time in intact femurs of both Pten-CKO and WT (slope=4.8, 95% CI: -1.9, 11.5, p=0.17). σ_{max} increased over time in callus femurs of both the Pten-CKO and WT femurs with a slope 10.7 units higher than intact femurs (95% CI: 1.3, 20.1, p=0.036). For all days PF, σ_{max} of the callus femurs of both the Pten-CKO and WT were significantly less than intact femurs (RM-ANOVA p<0.001). By day 28 PF, σ_{max} in callus Pten-CKO and WT femurs were 63% and 62% less than their corresponding intact femurs, respectively.

c. Minimum section modulus, z_{min}, versus days PF, with 95% CIs labeled. z_{min} did not change with days PF for any of the groups (p=0.56). z_{min} of intact and callus Pten-CKO femurs were nearly twice as large as their respective WT counterparts for all days PF. Further, callus femurs of both Pten-CKO and WT were more than twice as large as their respective contralateral intact femurs.

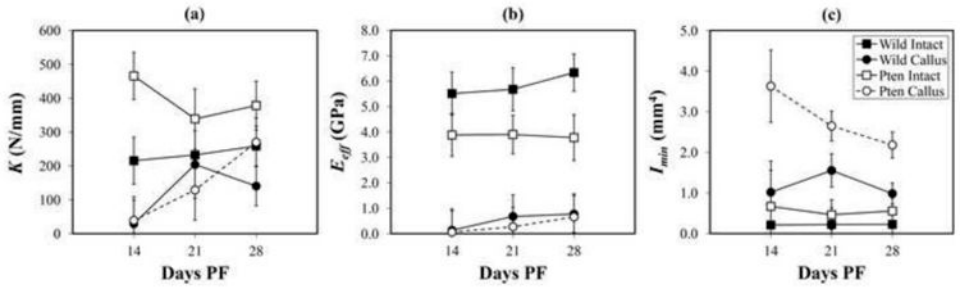

Figure 5.

a. Bending stiffness, *K*, versus days PF, with 95% CIs labeled. *K* of callus Pten-CKO femurs increased with time such that a 587% increase was found between days 14 and 28 PF (p=0.010). In contrast, no significant change in *K* of callus WT femurs was found over the course of the study. *K* of callus WT femurs were significantly less than their corresponding intact bones at 28 days PF (p=0.034). In contrast, no significant difference was found between *K* of callus and intact Pten-CKO femurs at 28 days PF.

b. Effective flexural modulus, E_{eff}, versus days PF, with 95% CIs labeled. E_{eff} increased with time in both callus Pten-CKO and WT femurs (p=0.002). E_{eff} of callus femurs was significantly smaller than their respective intact femurs for all days PF ($p<0.05$). No significant differences were found between callus Pten- CKO and callus WT femurs over the course of the study. In contrast, E_{eff} of intact Pten-CKO femurs was significantly smaller than intact WT femurs at 28 days PF ($p<0.05$).

c. Minimum second moment of area, I_{min}, versus days PF, with 95% CIs labeled. No changes were found in I_{min} over the duration of the experiment in any of the groups (p=0.15). I_{min} of intact and callus Pten-CKO femurs were significantly larger than their respective WT counterparts ($p<0.05$); and, I_{min} of callus femurs of both Pten-CKO and WT were significantly larger than their respective contralateral intact femurs ($p<0.05$).

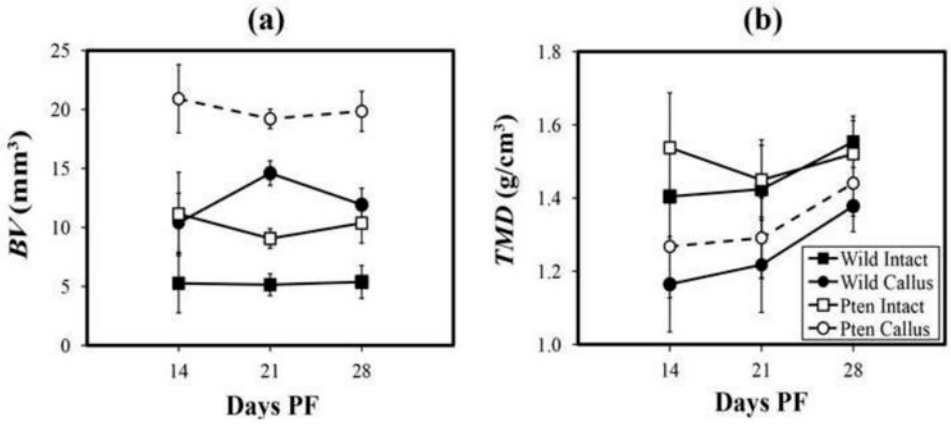

Figure 6.

a. Bone volume, *BV*, versus days PF, with 95% CIs labeled. No changes were found in *BV* over the duration of the experiment in any of the groups (p=0.85). *BV* of intact and callus Pten-CKO femurs were nearly twice their respective WT counterparts at 28 days PF (p<0.01); and, *BV* of callus femurs of both Pten-CKO and WT were roughly twice their respective contralateral intact femurs (p<0.01).

b. Tissue mineral density, *TMD*, versus days PF, with 95% CIs labeled. *TMD* of intact femurs of both Pten-CKO and WT was found to significantly increase with time (slope 0.06, 95%: 0.01, 0.10, p=0.019). *TMD* of callus femurs of both Pten-CKO and WT significantly increased with time with a slope 0.04 units larger than intact femurs (95% CI: 0.02, 0.07, p=0.005). *TMD* of callus Pten-CKO femurs was significantly less than contralateral intact femurs at 14 and 21 days PF (p=0.009, p=0.010, respectively). *TMD* of callus WT femurs of the was significantly less than their respective contralateral intact femurs for all days PF (p=0.002, p=0.010, p=0.002, respectively).

Table 1

Summary of the Number of Samples Mechanically Tested in Four-Point Bending and Analyzed with the μCT Image-Based Method for the Present Study

Mouse	Femur	Total		14 days PF		21 days PF		28 days PF	
		Mechanically Tested	μCT	Mechanically Tested	μCT	Mechanically Tested	μCT	Mechanically Tested	μCT
WT	Intact	13	14	3	4	4	4	6	6
	Callus	13	14	3	4	4	4	6	6
Pten-CKO	Intact	12	12	3	3	5	5	4	4
	Callus	12	12	3	3	5	5	4	4